Inorganic Chemistry

Article

pubs.acs.org/IC

Mechanism of the *cis*-[Pt(1*R*,2*R*-DACH)$(H_2O)_2]^{2+}$ Intrastrand Binding to the Double-Stranded (pGpG)·(CpC) Dinucleotide in Aqueous Solution: A Computational DFT Study

Zdeněk Chval,*[,†] Martin Kabeláč,[‡] and Jaroslav V. Burda*[,§]

[†]Department of Laboratory Methods and Information Systems, Faculty of Health and Social Studies, University of South Bohemia, J. Boreckého 27, 370 11 České Budějovice, Czech Republic

[‡]Department of Chemistry, Faculty of Science, University of South Bohemia, Branišovská 31, 37005 České Budějovice, Czech Republic

[§]Department of Chemical Physics and Optics, Faculty of Mathematics and Physics, Charles University, Ke Karlovu 3, 121 16 Prague 2, Czech Republic

Supporting Information

ABSTRACT: A mechanism of the intrastrand 1,2-cross-link formation between the double-stranded pGpG·CpC dinucleotide (ds(pGpG)) and fully aquated oxaliplatin *cis*-[Pt(DACH)$(H_2O)_2]^{2+}$ (DACH = cyclohexane-1*R*,2*R*-diamine) is presented. All structures of the reaction pathways including the transition states (TSs) were fully optimized in water solvent using DFT methodology with dispersion corrections. Both 5′ → 3′ and 3′ → 5′ binding directions were considered. In the first step there is a slight kinetic preference for 5′-guanine (5′G) monoadduct formation with an activation Gibbs free energy of 18.7 kcal/mol since the N7 center of the 5′G base is fully exposed to the solvent. On the other hand, the N7 atom of 3′-guanine (3′G) is sterically shielded by 5′G. The lowest energy path for formation of the 3′G monoadduct with an activation barrier of 19.3 kcal/mol is connected with a disruption of the 'DNA-like' structure of ds(pGpG). Monoadduct formation is the rate-determining process. The second step, chelate formation, is kinetically preferred in the 3′ → 5′ direction. The whole process of the platination is exergonic by up to −18.8 kcal/mol. Structural changes of ds(pGpG), charge transfer effects, and the influence of platination on the G·C base pair interaction strengths are also discussed in detail.

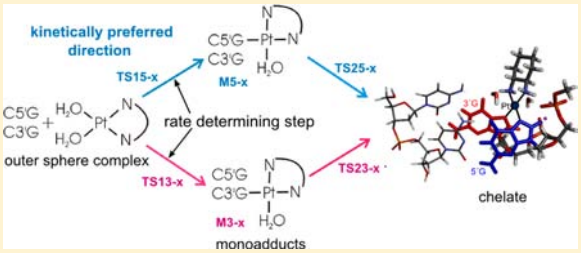

INTRODUCTION

Discovery of antitumor activity of cisplatin by Rosenberg more than 40 years ago[1] started an extended study of the chemical and biological properties of platinum compounds. Cisplatin is a very efficient drug against ovarian, bladder, head, neck, as well as nonsmall lung and cervical cancers. However, its use has several limitations such as severe side effects and the possibility of intrinsic and acquired resistance promoting the search for new, less toxic, and more efficient drugs.

Oxaliplatin [(cyclohexane-1*R*,2*R*-diammine)oxalatoplatinum-(II)] is a third-generation platinum drug,[2] which is active against some cisplatin-resistant tumors[3] and has a lower overall toxicity than cisplatin. In oxaliplatin, the two ammine and chloro ligands of cisplatin are replaced by the bidentate DACH and oxalate group ligands (Figure 1). Oxaliplatin forms similar adducts with DNA as cisplatin; however, adduct affinity toward proteins may be different for the two drugs.[4] On the other hand, the oxalate leaving group changes the rate of aquation[5] and cellular uptake of the drug.[6] Biotransformation of oxaliplatin was recently reviewed by Jerremalm et al.[7] In the blood oxaliplatin reacts rapidly with proteins and sulfur-containing compounds like methionine and glutathione, but the resulting adducts are probably noncytotoxic. Oxaliplatin can be also rapidly hydrolyzed, establishing an equilibrium between intact oxaliplatin and the highly reactive oxalato monodentate [Pt(DACH)(oxalate)(H_2O)] complex.[8] However, whether this complex represents the active form of oxaliplatin which reacts with DNA is to the best of our knowledge unknown.

In the simpler case of cisplatin there is a general agreement that the partially aquated $[Pt(NH_3)_2Cl(H_2O)]^+$ complex is the active form of the drug which interacts with DNA.[9−11] However, it is still not clear to what extent $[Pt(NH_3)_2Cl(H_2O)]^+$ reacts with DNA forming covalently bound monoadducts since according to an alternative mechanism $[Pt(NH_3)_2Cl(H_2O)]^+$ forms an outer-sphere complex with DNA.[12] Then a specific local DNA microenvironment may speed up substantially the second aquation step and suppress formation of $[Pt(NH_3)_2(OH)(H_2O)]^+$ from $[Pt(NH_3)_2(H_2O)_2]^{2+}$ (its pK_a value is ca. 5.5[13,14] in the 'bulk' water solution). Thus, the most reactive and fully aquated $[Pt(NH_3)_2(H_2O)_2]^{2+}$ complex could be the species that forms a

Received: December 4, 2012
Published: May 8, 2013

   dx.doi.org/10.1021/ic302654s | *Inorg. Chem.* 2013, 52, 5801−5813

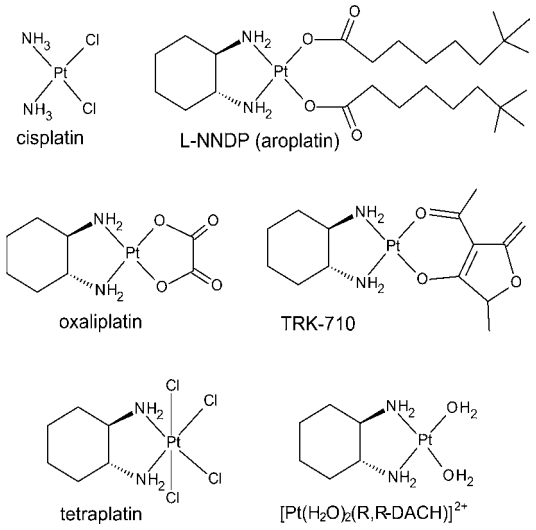

Figure 1. Structures of cisplatin, oxaliplatin, some other DACH-containing drugs which entered to clinical trials,[15] and the fully aquated form $[Pt(H_2O)_2(R,R\text{-DACH})]^{2+}$ that is considered in this study.

covalent bond with the N7 atom of guanine.[12] According to the cited paper the hydrogen bond (H-bond) interactions play an important role in stabilization of the transition state for monoadduct formation, and the rate of platination is given by the H-bond donor ability of the ligands of the Pt(II) drug.[12] If these assumptions are correct then the diaqua $[Pt(R,R\text{-DACH})(H_2O)_2]^{2+}$ complex may have an even more important impact on the reactivity of Pt(DACH) complexes than the $[Pt(NH_3)_2(H_2O)_2]^{2+}$ hydrated form for cisplatin since some H-bond acceptor centers on DNA may be inaccessible for the bulkier DACH ligand. This increases the relative importance of the leaving group ligands as H-bond donors. Thus, we believe that our model represented by the fully aquated $[Pt(R,R\text{-DACH})(H_2O)_2]^{2+}$ complex, and the ds(pGpG) dinucleotide may offer useful insight into the DNA binding mechanism of oxaliplatin and other DACH-containing drugs (Figure 1).

It is known that 60−65% of cisplatin is bound to GpG sites.[16] Experimental results show that the rate of platination is higher for double-stranded oligonucleotides than for single-stranded ones,[3,17,18] and it increases with the length of the oligonucleotide.[19] This is probably caused by an enhanced diffusion due to electrostatic attraction between a higher number of the negatively charged phosphate groups and the positively charged (aquated) Pt(II) drug.[17]

Monofunctional adducts are formed faster with 5′G than 3′G in the GG sequences.[3,4,6] On the other hand, in the AG/GA sequence context intrastrand 1,2-AG cross-links are formed (representing 20−25% of all platinum adducts), while 1,2-GA chelates are hardly detectable despite very similar binding energies.[20] It suggests that cross-link formation should start uniquely on 3′G since the first platinum attack occurs always at a guanine base. Therefore, the exact place of the first platinum attack is clearly sequence dependent. Baik et al.[21] used pApG and pGpA single strands to model the AG and GA chelate formations, respectively. The AG chelate was formed preferably compared to the GA one due to transition state stabilization by an H-bond between the ammine and the 5′-phosphate (5′P) groups.[21] A detailed discussion about the mechanistic aspects of the platinum drugs' binding to DNA is presented in a review by Kozelka.[22]

There are a number of studies dealing with the mechanisms of the substitutions of aqua ligand(s) by one or two isolated guanine nucleobases in various activated (aquated) platinum square planar compounds.[23−30] Three basic conformations of the two guanine ligands have been recognized in product structures: one head-to-head (HH) and two head-to-tail conformations (ΔHT,ΛHT).[31] The HT conformations are energetically more feasible than the HH conformation.[26,31] However, only the HH conformation can be regarded for the intrastrand cross-link in double-stranded DNA (ds-DNA).

In this contribution the fully optimized stationary points for monoadduct formation of the $[Pt(H_2O)_2(R,R\text{-DACH})]^{2+}$ complex (labeled as PtDACH hereafter) with ds(pGpG) and for subsequent formation of the 1,2-GG chelate are presented. Both possible 5′ → 3′ and 3′ → 5′ binding directions (Figure 2) are considered. While structures of the stable monoadducts

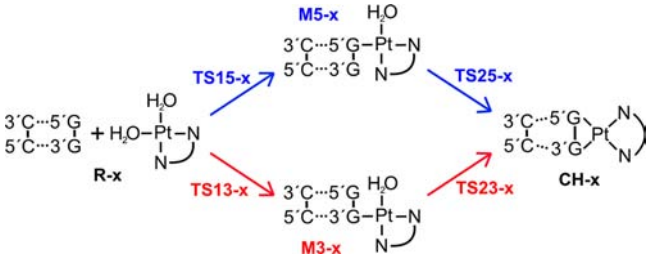

Figure 2. Platinum cross-linked structure with the GG sequence may be formed either via a 5′G-monoadduct (5′G → 3′G direction, blue) or via a 3′G-monoadduct (3′G → 5′G direction, red).

and chelates of the Pt(II) compounds with DNA have been studied in many theoretical as well as experimental studies,[4,32−48] fully optimized structures of all important structures (including the transition states) along both possible reaction pathways are published for the first time. Since the DACH amine groups have neither strong σ-donation nor strong π-back-donation ability it can be expected that substitution in both directions will follow an associative interchange mechanism[49] with elongated bonds to the entering and leaving ligands.[50] It is shown that steric hindrance and nonbonding interactions affect the structures of transition states and monoadducts, and in this way, they influence the energetics and specificity of the binding.

COMPUTATIONAL DETAILS

All geometries were fully optimized using the RI-TPSS-D/COSMO method, which comprises the TPSS functional[51] including the resolution of identity (RI) approximation of the Coulomb integrals, the empirical dispersion term for the main group elements,[52] and the COSMO continuum solvation model with the cavities constructed based on the Klamt's atomic radii[53] and water as the medium. The Coulomb potentials of all elements were approximated by auxiliary basis sets developed by Weigend.[54]

The TPSS-D functional is able to reproduce well the conformational changes and stacking interactions in nucleic acids and related systems.[55−57] Recently, a similar methodology was used also for description of transition metal compounds.[58,59] In the optimization model used in this study, the main group elements are described by a split valence def2-SV(P) basis set. The platinum atom was treated using Dresden−Stuttgart quazirelativistic energy-averaged effective pseudopotentials[60] with a pseudo-orbital basis set augmented by the set of diffuse (α_s = 0.0075, α_p = 0.013, α_d = 0.025) and polarization (α_f = 0.98) functions.[61] These calculations were performed by the Turbomole 6.1 program[62] and labeled as RI-TPSS-D/BSI/COSMO in

dx.doi.org/10.1021/ic302654s | Inorg. Chem. 2013, 52, 5801−5813

further text. Despite the fact that it is known[63] that combination of TPSS-D with a DZ basis set generally leads to slightly underestimated H-bond distances, we found that the RI-TPSS-D/BSI/COSMO method offers very good geometries of Pt(II) complexes and a reasonable description of the dispersion interactions (cf. below). Since the main structural changes during the PtDACH binding are connected with ligand substitutions on the Pt(II) center and unstacking of both guanines, this method represents in our opinion a reasonable compromise between applicability and accuracy.

All geometries were fully optimized with a tight converge maximum norm of the Cartesian gradient of 10^{-4} au and the DFT energy convergence criterion of 10^{-8} hartree. The nature of the obtained stationary points was always checked by a numeric evaluation of the Hessian matrix. Calculated frequencies were corrected by a default scaling factor of 0.9914. Thermal contributions to the energetic properties were calculated using the canonical ensemble at standard gas-phase conditions (T = 298 K, p = 101.325 kPa). We are aware of the fact that this approach is not completely consistent for the solvent-optimized structures,[64] but optimizations in the gas phase and subsequent Hessian evaluations would almost double the needed computational time.

Wave function properties and relative energies of the optimized structures were obtained by the ωB97XD/MWB-60(2f)/6-311+G-(2d,2p)/IEFPCM/UFF single-point calculations. The platinum atom was augmented by the set of diffuse functions in analogy to BSI and by the set of polarization functions (α_f = 1.419; 0.466). The main group elements were described by the 6-311G(2d,2p) basis set, and electronegative N, O elements were furthermore augmented by a set of diffuse functions (6-311+G(2d,2p) basis set). This basis set is designated as BSII in further text. These calculations were carried out by the Gaussian 09 (G09) program package[65] with the Integral Equation Formalism-PCM solvent model (IEFPCM and UFF scaled radii for cavity construction). Atoms in molecules (AIM) topological analysis of the electron density in bond critical points was performed by the AIMAll program,[66] and natural population analysis (NPA) partial charges were determined by the NBO 3.1 program.[67] Structures were visualized, and structural properties were analyzed using the Molden, Gabedit, X3DNA, and Olex2 programs.[68−71]

In order to facilitate a comparison with the previous quantum chemical studies on guanine binding to platinum complexes calculated almost exclusively with the B3LYP functional;[21,23−26,29,30,72,73] single-point energy calculations were also performed at the B3LYP-D/MWB-60(2f)/def2-TPZVPP/COSMO level by the Turbomole 6.1 program. This basis set is labeled as BSIII in further text.

Solvent-phase interaction energies ΔE^{wat}_{INT} were calculated at the ωB97XD/BSII/IEFPCM level for two different sets of fragments: [pGpG(PtDACH) = pGpG(Pt) and CpC] and [ds(pGpG) and PtDACH] as the differences between the total energies of the complexes and the energies of the given fragment sets. Obtained values have been corrected for the basis set superposition error (BSSE) using the standard counterpoise method.[74] In calculations of BSSE corrections within the PCM regime, the ghost atomic orbital functions were localized inside the cavity, which has the same size as the whole complex. Such a model was described in our previous study.[75]

For the interaction of the pGpG(Pt) and CpC fragments in the minimum structures also solvent-phase pairing energies ΔE^{wat}_{PAIR} were calculated from ΔE^{wat}_{INT} considering deformation energies ΔE^{i}_{def} of the fragments

$$\Delta E^{wat}_{PAIR} = \Delta E^{wat}_{INT} + \sum_i \Delta E^{i}_{def} \quad (1)$$

Additional single-point calculations on selected optimized structures were conducted using the Amsterdam Density Functional 2008.1 package (ADF)[64] to calculate fragment energy decompositions according to the extended transition state theory[76,77] combined with natural orbitals for chemical valence (ETS-NOCV).[78−80] Gas-phase interaction energies ΔE^{gas}_{INT} (not corrected for the BSSE error) were decomposed to Pauli (ΔE_{Pauli}), electrostatic (ΔE_{elstat}), orbital (ΔE_{orb}), and dispersion (ΔE_{disp}) energy contributions

$$\Delta E^{gas}_{INT} = \Delta E_{Pauli} + \Delta E_{elstat} + \Delta E_{orb} + \Delta E_{disp} \quad (2)$$

In these calculations, scalar relativistic effects were treated within the zeroth-order regular approximation (ZORA).[81,82] The TPSS-D functional was used with the all-electron TZ2P (ZORA) basis set for all atoms.

RESULTS AND DISCUSSION

Model Preparation. ds-DNA was simulated by the double-stranded pGpG·CpC dinucleotide (ds(pGpG)). The initial structure was generated in the ideal B-DNA conformation by the NAB program, which is a part of the AmberTools package. The negative charge of the phosphate groups was compensated by three Na^+ ions. The terminal 5′-phosphate group (5′P) on the pGpG strand stabilizes the DNA adducts with cisplatin-like drugs.[21,83] In the first step the 5′P group was kept fixed when optimizing the rest of the system to ensure a reasonable starting conformation of 5′P for a structural alignment of ds(pGpG) with the PtDACH complex.

Different starting conformations between the ds(pGpG) and the PtDACH subunits were considered where the two subunits were associated by the H-bonds to each other. The N7 and O6 atoms of 5′G and 3′G together with 5′-phosphate oxygens O(5′P) of the pGpG strand were considered as H-bond acceptors. The two H_2O ligands and two H_2N- groups of PtDACH were involved as H-bond donors. Resulting structures were fully optimized to obtain "reactant" structures. The two lowest reactants **R-1** and **R-2** (Figures 3 and 4) were chosen for exploration of the reaction mechanism.

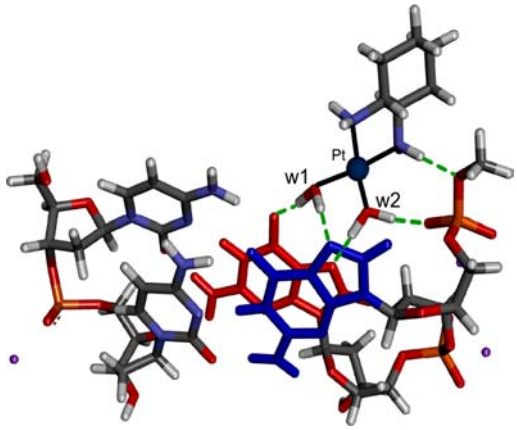

Figure 3. Structure of **R-1** with the designation of water ligands w1 and w2. 5′G and 3′G are colored in blue and red, respectively. Coordination bonds of the Pt atom and selected H-bonds are represented by the solid black and dashed green lines, respectively.

Structures with the H-bonds between the N7(3′G, 5′G) atoms and the H_2N- groups of DACH were not energetically feasible due to close contacts between ds(pGpG) and the bulky DACH ligand, which lead to severe deformations of the pGpG strand. All structures were by at least 7.6 kcal/mol higher in energy than the most stable reactant structure **R-1** and therefore are not considered in this study. Clearly, more H-bond patterns would be possible for cisplatin with much smaller ammine ligands than for oxaliplatin with the bidentate DACH ligand. Structural parameters of **R-1** are summarized in Tables 1, 2, and S1, Supporting Information. **R-1** is stabilized by five strong H-bonds (Figure 3) with a total interaction energy of −65.9 kcal/mol between the ds(pGpG) and the PtDACH

dx.doi.org/10.1021/ic302654s | Inorg. Chem. 2013, 52, 5801−5813

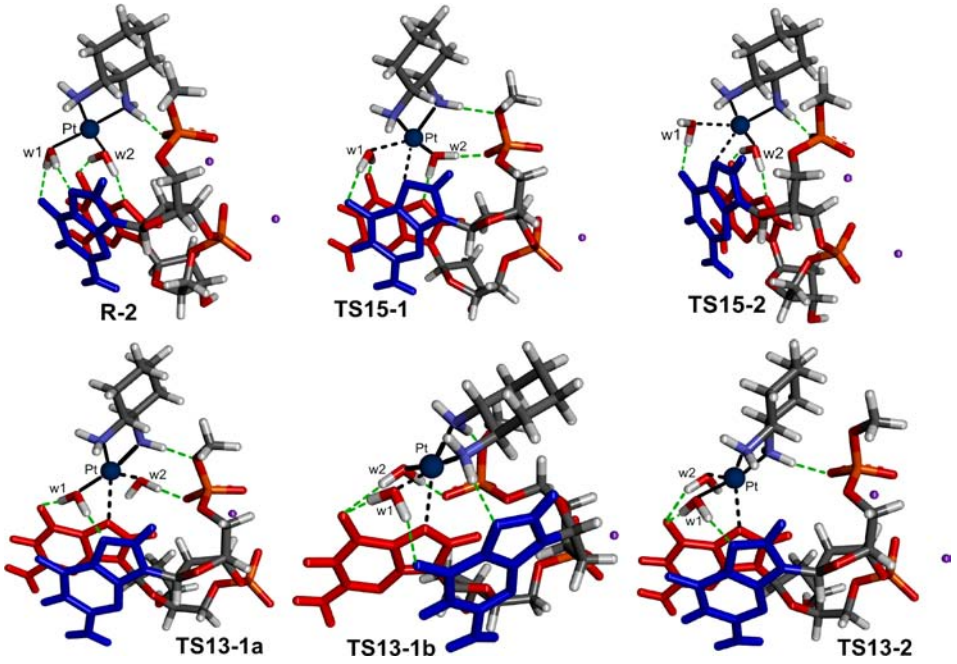

Figure 4. Structures of **R-2** and transition states for monoadduct formation. CpC strand is not shown for clarity. Pt−entering ligand and Pt−leaving ligand bonds are shown by the black dashed lines. 5′G and 3′G are colored in blue and red, respectively. Coordination bonds of the Pt(II) atom and selected H-bonds are represented by the solid black and dashed green lines, respectively.

Table 1. Main Bonding Distances for Selected Structures and Geometric Parameters That Describe the Mutual Position of the Pt(II) Complex with the Planes of 5′G and 3′G[a]

structure	Pt−N7(5′G)	Pt−N7(3′G)	Pt−O(w1)	Pt−O(w2)	Pt−5′G distance[b]	Pt−3′G distance[b]	PtDACH−5′G angle[c]	PtDACH-3′G angle[c]
R-1	3.844	4.206	2.059	2.043	3.455	0.338	39.7	38.4
R-2	3.457	4.345	2.085	2.044	2.978	0.431	62.6	68.0
TS15-1	2.468	4.139	2.366	2.057	1.896	1.323	60.3	60.0
TS15-2	2.391	4.283	2.456	2.050	1.901	1.082	74.1	76.2
TS13-1a	3.765	2.855	2.063	2.739	3.090	0.432	54.4	49.8
TS13-2	3.561	2.610	2.074	2.349	3.458	0.355	61.4	58.7
TS13-1b	4.170	2.440	2.455	2.087	3.997	1.157	74.5	81.1
M5	2.019	4.083	3.273	2.061	0.664	1.677	77.7	65.5
M5-w	2.021	3.985	n.a.	2.054	0.791	1.898	79.9	76.8
M3-1a	3.658	2.037	2.070	4.244	3.628	0.462	56.9	50.7
M3-2	3.404	2.035	2.066	3.165	3.176	0.337	47.2	45.6
M3-2-w	3.457	2.034	2.068	n.a.	3.226	0.338	45.9	49.5
TS25	2.040	2.581	3.465	2.403	1.012	1.339	80.0	87.5
TS25-w	2.025	2.405	n.a.	2.491	1.001	1.549	78.8	90.0
TS23	2.419	2.026	2.421	4.119	2.057	0.203	74.4	67.0
TS23-w	2.400	2.022	2.427	n.a.	2.044	0.262	74.3	65.4
CH5	2.058	2.032	3.095	3.658	1.398	0.599	69.9	71.1
CH5-w	2.062	2.048	n.a.	3.436	1.284	0.375	54.4	49.8
CH3	2.058	2.028	3.109	3.499	1.407	0.499	64.3	66.5
CH3-w	2.043	2.031	3.165	n.a.	1.125	0.658	70.5	69.8
OX-DNA (X-ray)[d]	1.98	1.94	n.a.	n.a.	1.37	0.83	68.4	67.2

[a]Distances are in Angstroms and angles in degrees. [b]Distance between the Pt atom and the mean plane of guanine (5′G or 3′G). [c]Angle between the mean planes of guanine (5′G or 3′G) and the Pt(II) complex. [d]Data based on analysis of the PDB structure 1IHH[45] by the Olex2 program.[71]

fragments (Table 3). Pt−N7(5′G) and Pt−N7(3′G) distances are 3.844 and 4.206 Å, respectively (Table 1). The two water ligands w1 and w2 have H-bond contacts with N7(5′G), O6(3′G) and N7(3′G), O(5′P), respectively. The flexible 5′P group is distorted having the β (C4′−C5′−O5′−P) dihedral angle of ∼100°, while in the native B-DNA the values of this angle are about 143° and 180° for the BII and BI forms, respectively.[84,85] Note, however, that the distribution of the β torsion values is significantly broadened in the DNA complexes, and values even below 80° are possible.[85] Besides formation of the H-bond between the NH_2 group and 5′P, the distortion of the β dihedral angle enables establishment of an additional strong H-bond interaction between w2 and 5′P (Figure 3).

dx.doi.org/10.1021/ic302654s | Inorg. Chem. 2013, 52, 5801−5813

Table 2. Changes of the DNA Parameters During Pt−DACH Binding

structure	shift	slide	rise	tilt	roll	twist	5′G−3′G angle
DNA (NMR)[93]	0.24	−1.55[a]			1.12	30.29	
DNA (QM/MM)[95]	0.87	−1.73	3.83	2.27	−1.02	36.16	
d(pGpG)	−0.08	−0.82	3.62	4.86	3.81	45.48	1.7
R-1	0.23	−0.94	3.56	7.47	6.66	46.24	1.9
R-2	0.26	−1.84	3.70	7.39	5.34	41.36	5.6
TS15-1	0.40	−1.42	3.65	8.76	6.76	42.02	0.3
TS15-2	0.15	−1.49	3.60	6.29	6.03	42.88	3.3
TS13-1a	1.15	−1.27	3.70	10.46	12.16	37.81	8.9
TS13-2	0.70	−1.22	3.56	8.42	7.79	40.25	2.8
TS13-1b	0.77	−2.77	4.29	12.46	11.73	39.86	10.9
M5	0.83	−2.57	4.20	11.06	14.73	38.28	12.3
M5-w	0.85	−2.14	3.71	10.21	11.98	38.1	5.4
M3-1a	0.88	−1.26	3.50	10.35	8.91	39.47	7.4
M3-2	1.09	−1.17	3.63	8.81	10.36	36.65	7.0
M3-2-w	1.07	−1.17	3.63	9.63	10.97	36.98	7.9
TS25	1.39	−1.59	3.88	10.22	15.06	34.41	11.8
TS25-w	1.45	−1.66	3.97	8.39	13.16	32.64	11.5
TS23	1.14	−1.68	3.72	9.69	17.83	35.99	18.8
TS23-w	1.10	−1.62	3.67	9.41	17.39	35.2	19.0
CH5	1.27	−1.66	3.80	10.84	20.94	36.28	24.0
CH5-w	1.45	−2.19	4.21	12.04	23.89	38.88	24.6
CH3	1.33	−1.81	3.85	11.75	22.02	37.57	24.3
CH3-w	1.26	−1.62	3.80	11.40	23.85	34.69	30.4
OX-DNA (X-ray)[b]	1.05	−1.73	3.44	1.43	21.89	34.59	25.0
OX-DNA (NMR)[93]	0.84	−1.36			28.30	25.20	35.6
OX-DNA(QM/MM)[95]	0.95	−1.60	3.34	−5.50	25.51	23.88	

[a]This value of the slide is typical for A-DNA rather than for B-DNA for which it should be much less negative. [b]Data based on analysis of the PDB structure 1IHH[45] by the X3DNA program.[70]

Table 3. Gas-Phase ΔE_{IE}^{gas} and Solvent-Phase ΔE_{IE}^{wat} Interaction Energies between the pGpG·CpC and the Pt(DACH) Fragments[a]

structure	ΔE_{Pauli}	ΔE_{elstat}	ΔE_{orb}	ΔE_{IE}^{gas}	ΔE_{IE}^{wat}	ΔE_{def}^{DNA}
R-1	90.7	−168.6	−103.1	−199.0	−65.9	1.0
R-2	96.0	−176.2	−95.2	−194.7	−59.0	2.6
TS15-1	116.8	−198.9	−99.5	−202.1	−59.2	1.0
TS15-2	126.8	−202.9	−95.4	−193.2	−51.8	2.5
TS13-1a	83.0	−164.53	−88.34	−190.0	−49.4	1.9
TS13-2	93.2	−176.4	−85.0	−191.5	−50.6	0.9
TS13-1b	122.7	−206.0	−101.4	−211.8	−59.0	5.3
M5	169.7	−261.2	−132.8	−241.4	−78.4	4.8
M3−1a	163.0	−254.5	−132.6	−245.4	−80.6	4.8
M3-2	183.3	−262.4	−138.3	−241.1	−80.0	2.6
TS25	158.8	−251.6	−125.9	−237.6	−67.0	7.0
TS23	188.0	−279.1	−140.1	−254.2	−75.8	8.4
TS23-w	188.9	−278.6	−138.2	−249.9	−74.5	7.9
CH5	204.7	−311.4	−171.9	−299.7	−94.2[b]	11.7
CH3	204.1	−309.3	−169.0	−299.1	−95.2[b]	10.7
CH3-w	204.3	−304.7	−171.4	−288.8	−91.6[b]	14.4

[a]Gas-phase interaction energies are decomposed to Pauli ΔE_{Pauli}, electrostatic ΔE_{elstat}, and orbital ΔE_{orb} energy contributions (eq 2). Deformation energies of the pGpG·CpC fragment ΔE_{def}^{DNA} are shown separately. Deformation energies of the Pt(DACH) fragment were not calculated since optimization of the metal complex without one or two ligands would lead to "imaginary" species with a substantially modified electronic configuration on the central cation, which is completely irrelevant to the original complex. All energies are in kcal/mol. [b]The value of −109.2 kcal/mol was calculated by the RI-B97-D/def2-TZVP/COSMO method (BSSE not included) for a similar system in ref 95.

Since a strong w2···5′P H-bond may hamper binding of PtDACH to 3′G the **R-2** structure was optimized where this H-bond was disrupted and replaced by the w2···O6(3′G) interaction. Nevertheless, the **R-2** structure appeared to have a less advantageous network of H-bond interactions compared to **R-1** (Figure 4, Table S2, Supporting Information, cf. the interaction and orbital interaction energies in Table 3), and consequently, the **R-2** reactant is 6.0 kcal/mol less stable than **R-1**. It means that according to the Boltzmann equilibrium distribution the population of **R-2** would be practically zero compared to **R-1**. For a longer DNA sequence the attainability of **R-1** is unclear (see above) and therefore **R-2** can be considered as the starting structure for alternative mechanisms of monoadduct formation in a more realistic model of natural ds-DNA. However, if not explicitly written, the relative energies of all structures described in this paper will be given with respect to **R-1**.

Monoadduct Formation. *Mechanisms Starting from R-1.* Nucleophilic attack of N7(5′G) on the Pt(II) center proceeds to the **TS15-1** transition state with the standard geometry of a trigonal bipyramid (Figure 4). In **TS15-1**, the N7(5′G) center is not sterically shielded by the 3′G base. The two bonds toward the leaving and entering groups are elongated by 0.31 and 0.45 Å with respect to stable Pt−O and Pt−N bonds in the reactant and product structures, respectively (Table 1). The activation Gibbs free energy barrier is 18.7 kcal/mol (Table 4).

Reaction of the PtDACH complex with the N7(3′G) center is much more complicated. We considered both water ligands w2 and w1 as possible leaving groups with corresponding **TS13-1a** and **TS13-1b** transition states, respectively.

dx.doi.org/10.1021/ic302654s | Inorg. Chem. 2013, 52, 5801−5813

Table 4. Gibbs Free Energy Reaction Profile of the Binding Reactions of the $[Pt(H_2O)_2(DACH)]^{2+}$ Complex to ds(pGpG) in the 5′ → 3′ and 3′ → 5′ Directions Calculated at the ωB97XD/IEFPCM/BSII//RI-TSSE-D/COSMO/BSI Level (in kcal/mol)[a]

5′ → 3′		5′ → 3′ (alternative)		3′ → 5′		3′ → 5′ (DNA deformed)		3′ → 5′ (alternative)	
R-1	0.0	**R-2**	6.0	**R-1**	0.0	**R-1**	0.0	**R-2**	6.0
TS15-1	18.7	**TS15-2**	23.2	**TS13-1a**	27.5	**TS13-1b**	19.3	**TS13-2**	24.7
M5-1	−7.7	**M5-2**	0.1	**M3-1a**	−4.5	**M3-1b**	−0.5	**M3-2 = M3-2-w**[b]	−8.8
TS25	16.4			**TS23**	12.4			**TS23-w**	13.6
CH5	−14.7			**CH3**	−18.8			**CH3-w**	−6.3

[a]See Table S6, Supporting Information, for B3LYP-D/BSIII/COSMO//RI-TSSE-D/BSI/COSMO energies. [b]The structure **M3-2-w** is considered to be equivalent to the structure **M3-2**. In **M3-2-w**, the released water molecule w1 is missing as compared to **M3-2** (see the text).

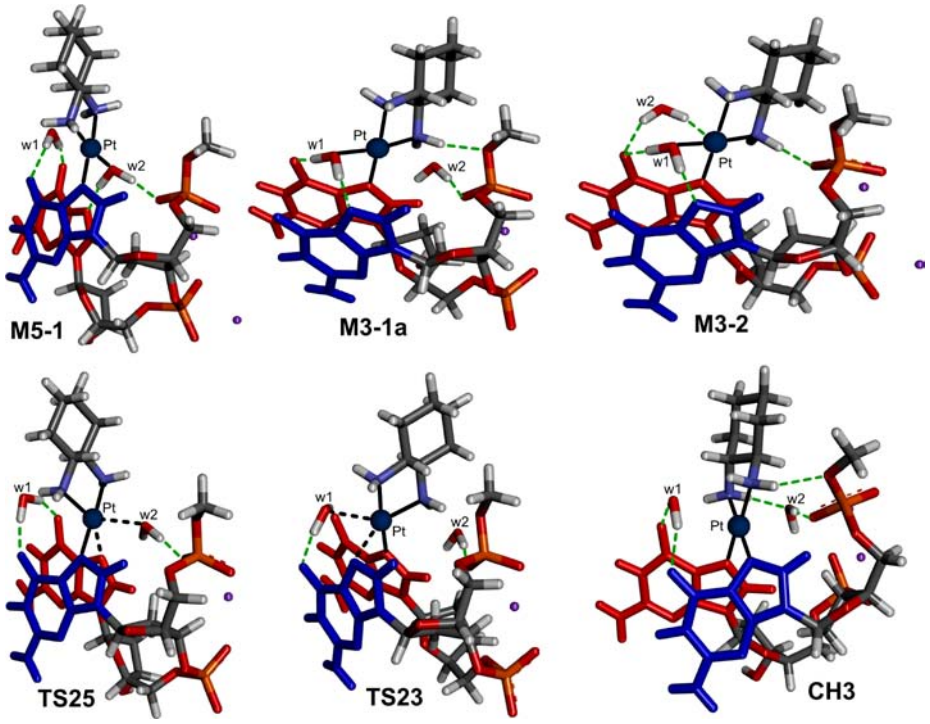

Figure 5. Geometries of monoadducts, TS structures for the chelate formation step, and **CH3** chelate. CpC strand is not shown for clarity. Pt−entering ligand and Pt−leaving ligand bonds are shown by the black dashed lines. 5′G and 3′G are colored in blue and red, respectively. Coordination bonds of the Pt(II) atom and selected H-bonds are represented by the solid black and dashed green lines, respectively.

In the **TS13-1a** transition state structure, all H-bonding interactions described in the **R-1** structure are preserved except the w2···N7(3′G) interaction that is replaced by an incipient Pt−N7(3′G) covalent bond (Figure 4). Due to the spatial orientation of both nucleobases (steric shielding by 5′G) the structure of **TS13-1a** is almost planar, the angle between the plane [Pt, N7(3′G) atom from entering and O(w2) from leaving ligands] and the plane of the Pt(II) complex [Pt and N atoms of the ammine groups] is only 10.2° (cf. Figure 4). Also, 5′P forms a strong H-bond with w2, decreasing the conformational freedom of the PtDACH complex since the leaving w2 ligand is kept tightly bound to the phosphate oxygen (cf. Figure 4). The enforced planarity of all Pt bonds in **TS13-1a** increases the repulsion between the ligands, which causesleads to a more dissociative nature of the Pt−N7(3′G) and Pt−w2 bonds compared to the Pt−N7(5′G) and Pt−w1 bonds in **TS15-1a** (Table 1), respectively. It leads to the increase of activation free energy up to 27.5 kcal/mol.

The isolated ds(pGpG) dinucleotide is much more flexible than the corresponding segment incorporated in a longer DNA chain. This increased flexibility enables formation of **TS13-1b**, where the leaving water molecule w1 established the H-bond with O6(5′G). The N7(5′G) site interacts with the H_2N group of DACH (see Figure 4). The Pt(II) coordination sphere of **TS13-1b** has almost an ideal geometry of a trigonal bipyramid with relatively short Pt−N7(3′G) and Pt−w1 distances of 2.440 and 2.455 Å, respectively. The PtDACH complex is nestled against the sugar−phosphate backbone of the pGpG strand, which is enabled by a strong bending of 5′P expressed by a very low value of the glycosyl bond torsion angle χ (89.1°). A normal conformation with χ between 200° and 300°[84] would lead to a steric clash between 5′P and DACH. Therefore, we expect that the **TS13-1b** structure is not transferable to the real DNA environment. However, it represents kinetically the most advantageous pathway for N7(3′G) monoadduct formation with an activation free energy barrier of 19.3 kcal/mol. Note that this value is still 0.6 kcal/mol higher than for the platinum binding to N7(5′G) represented by **TS15-1**. The pathway over **TS13-1b** leads to the fairly distorted (and unstable) **M3-1b** monoadduct structure (cf. Figure S1, Supporting Information).

Monoadduct formations of **M5-1**, **M3-1a**, and **M3-1b** are exergonic by −7.7, −4.5, and −0.5 kcal/mol, respectively. Due to similar structural features as **TS13-1b** (see above) we assume that **M3-1b** is also not transferable to real DNA. Summing up

dx.doi.org/10.1021/ic302654s | Inorg. Chem. 2013, 52, 5801−5813

Table 5. Gas-Phase Interaction Energies ΔE_{IE}^{gas} (eq 2) and Solvent-Phase Interaction ΔE_{IE}^{wat} and Pairing Energies ΔE_{PAIR}^{wat} (eq 1) between the pGpG(Pt) and the CpC Fragments[a]

structure	ΔE_{Pauli}	ΔE_{elstat}	ΔE_{orb}	ΔE_{IE}^{gas}	ΔE_{IE}^{wat}	$\Delta E_{def}^{pGpG(Pt)}$	ΔE_{def}^{CC}	ΔE_{PAIR}^{wat}
pGpG·CpC	89.6	−102.5	−47.1	−77.9[b]	−43.7	7.9	3.2	−32.6
R-1	91.8	−117.5	−54.4	−99.1	−46.2	8.0	2.7	−35.5
R-2	88.9	−117.4	−50.5	−98.4	−47.1	7.0	2.6	−37.6
TS15-1	90.5	−117.2	−51.9	−98.2	−46.9		2.4	
TS15-2	89.8	−118.1	−53.5	−101.3	−47.2		2.6	
TS13-1a	92.7	−118.3	−53.0	−97.4	−46.6		2.9	
TS13-2	94.3	−122.0	−57.5	−104.4	−47.5		2.7	
TS13-1b	97.9	−125.4	−51.2	−102.9	−48.9		2.4	
M5	95.4	−121.9	−50.6	−101.1	−48.4	6.9	2.3	−39.2
M3-1a	94.4	−122.5	−55.8	−103.0	−47.7	7.5	2.8	−37.4
M3-2	94.4	−122.3	−57.4	−104.1	−48.3	8.4	3.0	−36.9
TS25	89.2	−116.5	−50.2	−98.3	−46.0		2.0	
TS23	91.5	−120.6	−53.9	−102.7	−48.0		2.4	
TS23-w	91.3	−120.8	−54.1	−102.9	−48.0		2.5	
CH5	91.8	−121.5	−54.4	−104.1	−48.4	14.8	2.4	−31.2
CH3	91.3	−121.4	−53.1	−103.5	−48.5	9.2	2.3	−37.0
CH3-w	90.8	−119.7	−52.8	−101.6	−48.1	18.1	2.4	−27.6

[a]Deformation energies $\Delta E_{def}^{pGpG(Pt)}$ are calculated only for the stable minimum structures. All energies are in kcal/mol. [b]This value is in a good accord with previous theoretical data, which show that the energy of one G−C Watson Crick H-bond pair is −32.1 kcal/mol,[107] and interstrand base-stacking energies are −4.2 and −3.1 kcal/mol for the methylated 5′C_3′-3′_G5′ and 5′_C3′-3′G_5′ base pairs.[108]

this fact and the low stability of this structure we did not consider it for the subsequent chelation step. Despite the structural complexity of all intermediates, interconvertion of **M3−1b** into the more stable **M3-1a** structure can be expected to occur with a relatively low energy barrier.

M5-1 contains the stronger and shorter Pt−N7 bond of 2.019 Å compared to 2.037 Å in **M3−1a** (Tables 1 and S2, Supporting Information) as well as the larger bending of the planes of the two guanines (the GG angle) (Table 2). It is caused by the released w1 water molecule, which forms three H-bonds: two with the O6 atoms of the two guanines and one with the NH_2 group of DACH (the N−H···O distance is 1.867 Å) (Figure 5). If this water is removed from **M5-1**, the resulting **M5-1-w** structure (Figure S1, Supporting Information) is rather similar to **M5-1** except the much smaller GG angle and roll values (Table 2). No H-bond contacts were established between the DACH amino group and the O6 atoms of G's in **M5-1-w**, which is in agreement with the experimental evidence that O6 is probably a worse H-bond acceptor than water when forming an H-bond with the Pt−NH groups.[86,87]

*Mechanisms Starting from **R-2**.* The **R-2** reactant structure was also considered for the monoadduct formation step in both 3′G and 5′G binding directions with corresponding **TS13-2** and **TS15-2** transition states, respectively. **TS13-2** has a trigonal bipyramidal structure (Figure 4) with the Pt−N7(3′G) distance about 0.15 Å longer than the Pt−N7(5′G) bond in **TS15-1**. The reason is similar to that discussed in the case of **TS13-1a** but less pronounced. Again, the more dissociative character of **TS13-2** is probably caused by the interplay between the shielding of the N7(3′G) site by the adjacent 5′G base and the H-bond network of platinum complex ligands with O6(3′G), N7(5′G), and 5′P (Figure 4). With respect to **R-1**, the activation barrier is 24.7 kcal/mol, i.e., **TS13-2** is 2.8 kcal/mol lower than **TS13-1a** but lies 6.0 kcal/mol higher than **TS15-1**. Interestingly, with respect to **R-2** the barrier is as high as the activation from **R-1** to **TS15-1** (18.7 kcal/mol). Neverthless, N7(5′G) binding is kinetically preferred over N7(3′G) binding also in this case. Considering **R-2** as the reactant for N7(5′G) binding, the reaction proceeds over the **TS15-2** structure (Figure 4) with an activation barrier (with respect to **R2** reactant) of 17.2 kcal/mol. Thus, **TS15-2** is 1.5 kcal/mol more stable than **TS13-2**. **TS15-2** displays the shortest Pt−N7 distance for entering ligand (2.391 Å) from all TS structures (Table 1).

However, **M5-2** represents a distorted monoadduct structure (Figure S1, Supporting Information) with an endergonicity of +0.1 kcal/mol. Therefore, rapid relaxation of this structure into the much more stable **M5-1** structure can be expected. Furthermore, the H-bond pattern of the two structures differs only in the orientation of w2. In **M5-2**, both H-bonds between 3′G and w2 must be disrupted during the chelation step and then the reaction proceeds via the same (or very similar) TS structure as for **M5-1**. Thus, for subsequent chelate formation only the pathway starting from the **M5-1** structure is assumed.

M3-2 is the most stable monoadduct structure with an exergonicity of −8.8 kcal/mol with respect to **R-1**. Note the presence of the stabilizing (w2)O−H···Pt interaction (Figure 5), which was already reported in previous studies.[88−90] According to ETS-NOCV analysis this interaction contributes −6.9 kcal/mol to the orbital interaction energy of −138.3 kcal/mol between Pt(DACH) and ds(pGpG) fragments in the gas phase (Table 3). However, it was found that w2 is bound nonspecifically in **M3-2**. Therefore, w2 was removed and the **M3-2-w** structure (Figure S1, Supporting Information) used as the starting structure for the chelation step. The omitted w2 has a negligible influence on the structure of the monoadduct (cf. structural parameters of **M3-2** and **M3-2-w** in Tables 1, 2, and S1, Supporting Information; the RMSD of the two structures (heavy atoms) is 0.121 Å).

Chelate Formation. **M5-1**, **M3-1a**, and **M3-2-w** monoadducts were used as starting structures for chelate formation with **TS25**, **TS23-1**, and **TS23-2-w** transition states in the corresponding pathways. **TS25** has the highest activation free energy of 24.1 kcal/mol. It is caused by the more dissociative character of the incipient Pt−N7(3′G) bond (Figure 5), which is more than 0.15 Å longer than the Pt−N7(5′G) bond in

dx.doi.org/10.1021/ic302654s | Inorg. Chem. 2013, 52, 5801−5813

TS23-1 and **TS23-2-w** (Table 1). This results from the steric shielding of N7(3′G) by 5′G. Comparing **TS23-1** and **TS23-2-w** structures it can be seen (Table 4) that the former structure shows much lower activation energy (16.9 vs 22.4 kcal/mol), which is caused by the lower stability of the reference **M3-1a** structure compared to **M3-2-w**.

From the individual **TS25**, **TS23-1**, and **TS23-2-w** structures, the final chelates **CH5**, **CH3**, and **CH3-w** were obtained with reaction exergonicities of −14.7, −18.8, and −6.3 kcal/mol, respectively. The low stability of **CH3-w** is caused by the absence of any H-bond interactions between Pt(DACH) and 5′P (Figure S2, Supporting Information). **CH3-w** formation is in fact endergonic with respect to the corresponding monoadduct **M3-2-w** structure. On the other hand, the **CH5** and **CH3** chelates (Figures S2, Supporting Information, and 5, respectively) are significantly stabilized by several H-bonds: (1) between the NH_2 group of DACH and O6(3′G) and (2) involving 5′P: the weak direct NH_2···O′3-(5′P) interaction and the H-bonds mediated by the leaving water w2 molecule. This demonstrates an important role of 5′P in the thermodynamics of the chelation step.

CH5 and **CH3** differ mainly in the conformation of the pGpG sugar phosphate backbone, which is better relaxed in **CH3** than in **CH5** (cf. deformation energies ΔE_{def}^{DNA} and $\Delta E_{def}^{pGpG(Pt)}$ in Tables 3 and 5, respectively). Moreover, the Pt−N7(3′G) bond is slightly stronger in **CH3** (Tables 1 and S2, Supporting Information).

The geometry of the **CH3** chelate structure is very close to the crystallographic structure (PDB code 1IHH):[45] (1) The GG angle is 24.3° compared to 25° in the crystal (Table 2). The DNA environment and neighboring bases have probably only a small influence on the GG angle whose value is mainly a result of the interplay between the directionality of coordination covalent bonds in the Pt(II) cross-link and the Watson−Crick H-bonding with the complementary CpC strand. Note that the much higher GG angle value of 53.9° was found in the Pt(II) cross-link with the single-stranded pGpG sequence optimized by the RI-TPSS-D/BSI/COSMO method. Thus, the base pairing decreases the GG angle in the Pt(II) cross-links, and this decrease is accompanied by a distortion of the Pt atom from the 5′G plane (Table 1). (2) The NH_2 group also forms the H-bond to O6(3′G); the calculated distance is slightly longer compared to the crystal structure (3.2 vs 2.9 Å). The shortest distance between the nitrogen atom of the second DACH amino group and O6(5′G) is 4.7 Å, while in the crystal structure it is 4.4 Å.[45] This NH_2 group also forms a weak H-bond with water molecule w1, which spans the two O6 atoms. Such a water molecule was found in the high-resolution crystal structure of the cisplatin−DNA complex.[47] The displacement of the Pt atom from the 5′G and 3′G guanine planes is also rather similar for **CH3** and the crystal structure (see Table 1). The differences between the two structures can be mainly found in the puckering of sugar rings (Table S1, Supporting Information) and closer contacts of the DACH moiety with the 5′-phosphate in the **CH3** structure, which is caused by a larger conformational freedom of the terminal 5′P since it forms a free dangling end in our model.

In agreement with our previous study,[20] the Pt−N7(3′G) bond is stronger than Pt−N7(5′G) in all chelate structures (Table S2, Supporting Information), but unlike the cited study it is also shorter (Table 1). This is caused by geometric reasons since the Pt atom is much more displaced from the plane of 5′G than from the plane of 3′G (Table 1).

Energetics. Relative energies of all optimized structures calculated at the ωB97XD/IEFPCM/BSII and B3LYP-D/COSMO/BSIII levels are collected in Tables 4 and S6, Supporting Information, and final energy profiles are drawn in Figure 6. The latter method gives systematically higher values of activation energies and underestimates the strengths of Pt−N7 coordination bonds compared to the former method.

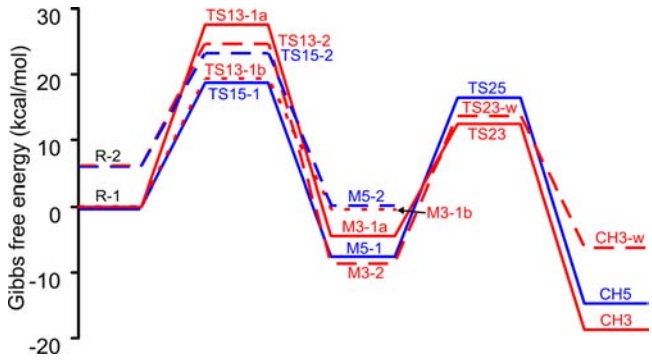

Figure 6. Gibbs free energy profiles of the binding reactions of the PtDACH complex to ds(pGpG) calculated at the ωB97XD/PCM/BSII//RI-TPSS-D/COSMO/BSI level (solid blue line, 5′G → 3′G direction; solid red line, 3′G → 5′G direction; long dashed blue line, an alternative mechanism for 5′G → 3′G direction; long dashed red line, an alternative mechanism for 3′G → 5′G direction; short dashed red line, a mechanism with a deformed dsDNA for 3′G → 5′G direction).

PtDACH binding is kinetically controlled by the first binding step (the monoadduct formation step), in agreement with experimental data for fully aquated cisplatin.[17] In the first step, N7(5′G) is slightly kinetically preferred over N7(3′G). The calculated B3LYP-D/BSIII activation barrier of 21.2 kcal/mol (**TS15-1**) is in a good agreement with the value of 21.4 kcal/mol published previously for binding of the fully aquated oxaliplatin with an isolated guanine.[72] This preference can be explained by the fact that the N7(5′G) center is fully exposed to the solvent in ds(pGpG), and the 3′G neighboring base does not influence the energetics of platinum monoadduct formation on N7(5′G).

On the other hand, binding to N7(3′G) is sterically hindered by 5′G. The reactivity of the most stable reactant **R-1** toward N7(3′G) is further decreased due to the w2···5′P H-bond stabilization. Thus, the conformational freedom of the entering and leaving ligands in the transition state region is decreased, leading to the almost planar **TS13-1a** structure. In this way, a disruption of either the 'DNA-like' structure of ds(pGpG) (as it occurs in **TS13-1b**) or the w2···5′P H-bond (in **TS13-2**) substantially decreases the activation free energy barrier.

A larger model is needed for a more realistic comparison of the N7(5′G) and N7(3′G) reactivities since in a longer DNA chain the N7(5′G) center will be also shielded by a neighboring nucleotide on its 5′-side.[91] The study with a larger model is currently under investigation.

Formation of the **M5**, **M3-1a**, and **M3-2** monoadducts is exergonic by −7.7, −4.5, and −8.8 kcal/mol, respectively. The latter two structures differ mainly in the position of the leaving water molecule w2. About 50% of the energy difference can be assigned to the larger deformation energy of the ds(pGpG) fragment in **M3-1a** compared to **M3-2** (Table 3).

In agreement with experimental data,[19] the chelation step is more favorable in the 3′G → 5′G direction overcoming a

dx.doi.org/10.1021/ic302654s | Inorg. Chem. 2013, 52, 5801−5813

barrier of 21.2 kcal/mol (**TS23** vs **M3-2**) than in the 5′G → 3′G direction where the activation barrier is by 2.9 kcal/mol higher (but the relative energy of **TS25** is 4.0 kcal/mol higher than **TS23**, Table 4). The whole process is exergonic but strongly dependent on established H-bond interactions. The most stable **CH3** structure lies 18.8 kcal/mol below the reactant **R-1** structure. More than 20% of this energy can be assigned to relaxation of the sugar phosphate backbone of the pGpG strand (the **CH5** → **CH3** transition, see above and Figure S2, Supporting Information).

Formation of one Pt−N7 dative bond increases the interaction energy between the ds(pGpG) and the Pt(DACH) fragments by about 15 kcal/mol in aqueous solution (Table 3), i.e., by about 30 kcal/mol in the chelates compared to **R-1**. In the gas phase this increase is about three times higher. Energy decomposition analysis in the gas phase shows that the difference is mainly caused by an increase of the orbital interaction energies since the change in the electrostatic contribution is to a large extent compensated by higher Pauli repulsion. Moreover, in water solvent the long-range electrostatic effects are essentially eliminated, while only the polarization part of the orbital interactions is affected to a larger extent compared to the gas phase.[92]

Changes of the ds(pGpG) Structure during the Cross-Link Formation. The ribose rings on the 5′G−3′C base pair remain almost always on the starting C2′-endo puckering (Table S1, Supporting Information), which is typical for B-DNA. On the other hand, the 3′G−5′C nucleotides (and especially 3′G ribose) show more pronounced changes in the pucker (Table S1, Supporting Information) probably due to the increased strain during cross-link formation. All helical parameters except the tilt follow trends observed in experiments,[45,47,93] molecular dynamics,[94] and QM/MM simulations.[95] The agreement with experimental results is good considering a large flexibility of the ds(pGpG) fragment. In comparison with ideal B-DNA, the two base pairs show increasing shift, negative slide, roll, and decreasing twist upon platinum binding (Table 2). The changes of these parameters are however not gradual for all structures along the reaction pathway, but local minima/maxima in their values may exist since these changes are driven by formation of the Pt−N7 bonds and H-bond interactions. For example, **M5-1** shows the highest value of negative slide due to the existence of the number of interactions between the PtDACH, the w2, and the ds(pGpG) fragments. Although the X3DNA program was not able to determine the form of the duplex for all structures, the transition from the B-DNA form toward A-DNA is apparent (Tables 2 and S1, Supporting Information), in agreement with experiments.[96]

Values of deformation energies for the ds(pGpG) fragment ΔE_{def}^{DNA} are shown in Table 3 and Figure 7. The ds(pGpG) fragment geometries in the reactant **R-x** and TS structures for the monoadduct formation step **TS1a-x** (a = 3, 5; x = 1a, 1b, 2) are only little affected by their interactions with the PtDACH complex. Starting from the monoadduct structures, the deformation energy ΔE_{def}^{DNA} gradually increases up to chelate values of ∼11 kcal/mol (Figure 7), and it reflects the changes of the GG angle (Figure 7). All important conformational changes of ds(pGpG) occur on the pGpG strand since the complementary CpC strand structure is almost unaffected by platination (see below).

GG-CC Base Pair Interaction Strength. In agreement with previous theoretical studies,[97,98] the strengths of the G−C

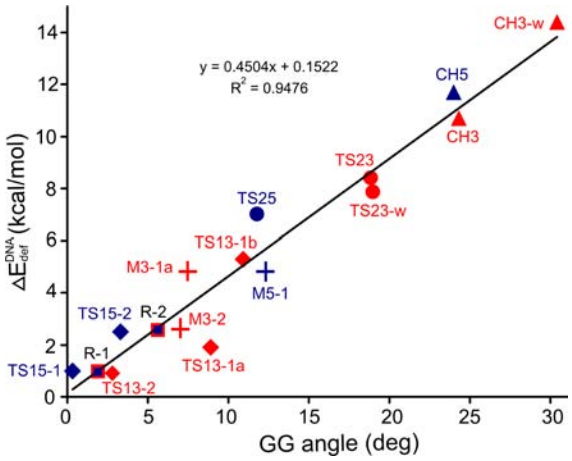

Figure 7. Roughly linear dependence of the ds(pGpG) deformation energy ΔE_{def}^{DNA} on the GG angle for the structures along the PtDACH binding pathways to ds(pGpG) (see Tables 2 and 3 for numeric values). Shapes of the points correspond to the positions of the structures on the reaction coordinate (■ → ◆ → + → ● →▲), and color refers to the binding direction (blue, 5′ → 3′; red, 3′ → 5′).

base pair interactions were tightened in the presence of the divalent platinum metal ion. Interaction and pairing energies between the platinated pGpG strand (pGpG(Pt)) and the CpC strand are shown in Table 5. The increase of the gas-phase interaction energies ΔE_{IE}^{gas} in **R-1** and **R-2** reactant structures with respect to the isolated ds(pGpG) complex is 21.2 and 20.5 kcal/mol, respectively. It is caused mainly by electrostatic interactions, which are however diminished to a large extent upon solvation. Thus, in aqueous solution the differences in pairing energies ΔE_{PAIR}^{wat} are lowered to 2.9 and 5.0 kcal/mol, respectively.

Formation of the covalent Pt−N7 bonds leads to additional enhancement of GG·CC interaction energies by up to 5% in both the gas phase and the water solvent as compared to **R-1** and **R-2** (Table 5). Thus, in the solvent enhancement is rather moderate and can be compensated by an increase of deformation energies of the pGpG(Pt) and CpC fragments in the platinated structures. The solvent-phase pairing energies ΔE_{PAIR}^{wat} range between −35.5 and −37.6 kcal/mol for most of the platinated structures, i.e., they are enlarged by about 10% with respect to the pGpG·CpC dinucleotide itself and do not visibly depend on the number of Pt−N7 bonds. The exceptions are **M5**, on the one hand, and the **CH5**, **CH3-w** structures, on the other, where lower and higher deformation energies of the pGpG(Pt) fragment affected the ΔE_{PAIR}^{wat} values being outside the above interval (Table 5). It should be stressed that the calculated deformation energies of the pGpG(Pt) fragment do not reflect the changes of DNA structure itself since they are calculated with respect to the minimized platinated single-stranded structures. Differences in deformation energies of the ds(pGpG) fragment itself are larger as follows from Table 3. The main structural changes occur only on the pGpG strand, and the deformation energies of the complementary CpC strand are very small and almost constant (Table 5).

Comparison of the H-bond strengths between the isolated GC pair and the different Pt(II) chelates was done by Robertazzi and Platts using AIM analyses.[99,100] In our model we observe also changes which occur in the course of chelate formation. The changes of electron densities in BCP's show that platination primarily weakens the strength of O6···H4

dx.doi.org/10.1021/ic302654s | Inorg. Chem. 2013, 52, 5801−5813

interactions since the two O6 atoms are involved in a direct H-bonding with the platinum ligands (Figure 8, Table S3, Supporting Information), which is in accord with our previous results.[101]

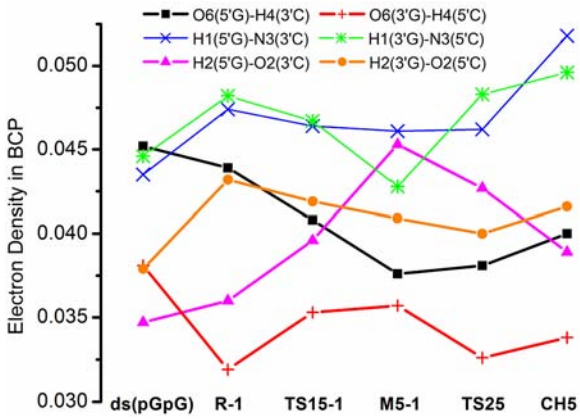

Figure 8. Electron densities in BCP's (in e/au^3) of the guanine–cytosine H-bonds for structures along the 5′G → 3′G direction of the PtDACH binding. See Table S3, Supporting Information, for values of other structures.

The changes in the BCP densities of the O6···H4 interactions can be used as an indirect measure of the strengths of the O6 interactions with PtDACH. For example in **R-1**, the O6(3′G) site serves as an H-bond acceptor in the strongest interaction with the w1 ligand of PtDACH compared to all other structures along the 5′ → 3′ pathway, which is demonstrated by the lowest electron density of 0.032 e/au^3 in BCP of the O6(3′G)···H4(5′C) H-bond, while for ds(pGpG) the corresponding value is 0.038 e/au^3 (Figure 8, Table S3, Supporting Information). On the other hand, the strength of the O6(5′G)···H4(3′C) H-bond is much less affected by the presence of PtDACH in **R-1**. Weakening of the O6···H4 interactions is compensated by the strengthening of the other two H1···N3 and H2···O2 H-bonds, where the platinated guanine serves as an H-bond donor. This effect was already reported in our previous studies.[97,102] Mainly the strength of the H2···O2 interactions inversely correlates with the strength of O6···H4 (Figure 8).

Charge Transfer Between PtDACH, pGpG, and CpC Fragments. In this section the charge transfer between the three fragments upon platination is described. To offer a more detailed picture, the pGpG fragment is further divided into the 5′G, 3′G, and GG-backbone subunits (Figure 9, Table S3, Supporting Information).

The charge transfer between PtDACH and DNA can be formally divided into three basic steps: the first one involves formation of **R-1** from originally two isolated PtDACH and (pGpG)·(CpC) molecules, which are connected by five H-bonds; the other two steps involve formation of the two donor–acceptor Pt–N7 bonds. In the first step the charge of −0.354 e is transferred from DNA to the drug; the net transferred charge is roughly proportional to a number of H-bonds, the charge of ca. −0.06 e per one H-bond. Thus, the largest charge of ca. −0.12 e is transferred from 3′G and GG-backbone subunits (Figure 9, Table S3, Supporting Information). Note that the charge transfer from the complementary CpC strand was enhanced by ca. −0.05 e compared to bare ds(pGpG).

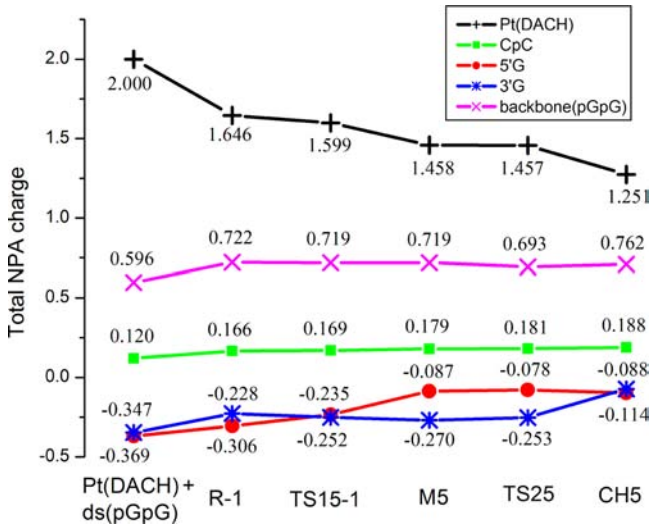

Figure 9. Changes of the NPA charges of the PtDACH, pGpG, and CpC fragments for structures along the 5′G → 3′G direction of the PtDACH binding. See Table S2, Supporting Information, for values of other structures.

Formation of the donor–acceptor Pt–N7 bonds is connected with the charge transfers of about −0.2 e per one established bond, and charge transfer should occur in the late stage of the Pt–N7 bond formation (i.e., after the transition state). Electron density of the other parts of the system is almost unaffected (cf. Figure 9, Table S3, Supporting Information).

Transferability of the Model into Longer DNA Chains. The ds(pGpG) structure represents a minimalistic model of DNA with the two guanine bases as reactive centers for platinum drug binding and the complementary CpC strand, which helps to keep the relative position of the two guanines close to that found in native DNA. Comparing experimental results for B-DNA and oxaliplatin–DNA chelates on one hand and our theoretical results for ds(pGpG) and **CH3** structures on the other we can make the following assumptions about limitations of our model and its transferability into longer DNA chains.

(1) The model is probably able to reproduce very well the changes in the GG angle upon platinum binding and reasonably well the changes in the helical parameters (except tilt), giving us confidence about a good description of the changes in the stacking interactions in the course of platinum binding (Table 2).

(2) The Pt(DACH) fragment with the bidentate DACH ligand is a rigid structure. In the chelate structures the position of this fragment is determined by the positions of the covalently bound N7 atoms of guanine bases (and vice versa). Thus, the geometry of the chelates is the least dependent on the flanking bases, and the geometry of the optimized chelate structures is in very good agreement with the crystal structure[45] (Table 1). However, going back to the reactants the conformational freedom between the pGpG·CpC and the Pt(DACH) fragments gradually increases. Thus, the orientation of the Pt(DACH) fragment with respect to ds(pGpG) is the most dependent on the nonbonding interactions in the reactant structures **R-1** and **R-2** showing the highest possible variability in longer DNA chains. Consequently,

dx.doi.org/10.1021/ic302654s | Inorg. Chem. 2013, 52, 5801–5813

the monoadduct formation step can be expected to be more influenced by the flanking bases than the chelate formation step. Depending on the sequence context the flanking bases may partially influence geometries, relative energies of the structures (Tables 4 and S6, Supporting Information), and interaction energies between Pt(DACH) and pGpG·CpC (or DNA) fragments (Table 3). Characteristics like, e.g., changes in interaction energies between the pGpG and the CpC fragments (Table 5) and charge transfer effects (Figure 9, Table S4, Supporting Information) will be affected only marginally. Deformation energies of the pGpG·CpC and pGpG(Pt) fragments (Tables 3 and 5) can be considered as the lower limit values for larger DNA fragments since deformation of DNA is not localized on the platinated GG sequence but also spread mainly to the 5′ flanking base pair step.[103,104] We believe that this study may provide useful reference data for more complex models, e.g., exploring the influence of flanking bases on both energetic and structural parameters connected with platinum drug binding.

(3) Some weakness of our model represents the free dangling 5′P group, which always adopts a conformation to form most advantageous contacts with the platinum complex. In this way the absolute values of interaction energies between the Pt(DACH) and the pGpG·CpC fragments (Table 3) are systematically overestimated for the structures along the reaction pathway for the mechanisms starting from the **R-1** structure. With this respect working with the relative energies of the structures we mostly relied on mutual cancellation of the errors. To overcome at least partially this problem the alternative mechanisms (starting from the **R-2** reactant) for both binding directions were also proposed in which the number of the H-bond contacts between the platinum complex and 5′P were reduced.

CONCLUSIONS

The mechanism of the $[Pt(H_2O)_2(DACH)]^{2}$ intrastrand binding to the ds(pGpG) sequence is presented with the fully optimized stationary points from the reaction coordinate. To the best of our knowledge, the results presented in this contribution offer the most realistic theoretical description of the course of the DNA platination available up to now. It enables us to describe not only the energetics of platinum binding but also the changes of the ds(pGpG) conformations, the influence of platination on the strengths of the G−C Watson−Crick base pairing, and the charge transfer effects. We show the importance of the transition state stabilization due to H-bond formation. The steric effects may also contribute to the transition state stabilization influencing mainly the strengths of the Pt−N7 bonds. A more dissociative nature of the incipient Pt−N7 bond in some TS structures is caused by close contacts between the Pt complex and the DNA molecule, distorting the trigonal bipyramidal geometry of the TS structure. In this way, the kinetics of platinum binding can be influenced by the flanking bases.[105] Our results support previous experimental evidence that Pt−N7 coordination is influenced mainly by the flanking bases from the 5′ side.[87,91,104,106] However, a larger model with more detailed insight into the structural relations between the stacked base pairs is necessary.

ASSOCIATED CONTENT

Supporting Information

Optimized structures of **M3-1b**, **M5-2**, **M5-1-w**, **M3-2-w**; optimized structures of **TS23-2-w**, **CH3-w**, **CH5** and structural alignment of structures **CH5** and **CH3**; sugar conformations of selected structures; values of electron densities in BCP's for the most important interactions between the Pt(DACH) and the ds(pGpG) fragments and H-bonds between pGpG(Pt) and CpC fragments; total NPA charges of fragments and selected atoms; base-pair parameters of selected structures; B3LYP-D/BSIII/COSMO//RI-TSSE-D/BSI/COSMO energies of the binding pathways; Cartesian coordinates of the optimized structures discussed in this paper. This material is available free of charge via the Internet at http://pubs.acs.org.

AUTHOR INFORMATION

Corresponding Author

*E-mail: chval@jcu.cz (Z.C.); burda@karlov.mff.cuni.cz (J.V.B.).

Notes

The authors declare no competing financial interest.

ACKNOWLEDGMENTS

This project was supported by grants from the Czech Science Foundation (project no. 208/12/0622) and from the Ministry of Education of the Czech Republic (MŠMT) (project ME 10149). Access to the MetaCentrum computing and storage facilities (grant LM2010005) is highly appreciated.

REFERENCES

(1) Rosenberg, B.; van Camp, L.; Krigas, T. *Nature* **1965**, *205*, 698−699.
(2) Mathe, G.; Kidani, Y.; Segiguchi, M.; Eriguchi, M.; Fredj, G.; Peytavin, G.; Misset, J.; Brienza, S.; Devassals, F.; Chenu, E.; Bourut, C. *Biomed. Pharmacother.* **1989**, *43*, 237−250.
(3) Rixe, O.; Ortuzar, W.; Alvarez, M.; Parker, R.; Reed, E.; Paull, K.; Fojo, T. *Biochem. Pharmacol.* **1996**, *52*, 1855−1865.
(4) Malina, J.; Novakova, O.; Vojtiskova, M.; Natile, G.; Brabec, V. *Biophys. J.* **2007**, *93*, 3950−3962.
(5) Lucas, M.; Pavelka, M.; Alberto, M.; Russo, N. *J. Phys. Chem. B* **2009**, *113*, 831−838.
(6) Zhang, S.; Lovejoy, K.; Shima, J.; Lagpacan, L.; Shu, Y.; Lapuk, A.; Chen, Y.; Komori, T.; Gray, J.; Chen, X.; Lippard, S.; Giacomini, K. *Cancer Res.* **2006**, *66*, 8847−8857.
(7) Jerremalm, E.; Wallin, I.; Ehrsson, H. *J. Pharm. Sci.* **2009**, *98*, 3879−3885.
(8) Jerremalm, E.; Eksborg, S.; Ehrsson, H. *J. Pharm. Sci.* **2003**, *92*, 436−438.
(9) Bancroft, D. P.; Lepre, C. A.; Lippard, S. J. *J. Am. Chem. Soc.* **1990**, *112*, 6860−6871.
(10) Davies, M. S.; Berners-Price, S. J.; Hambley, T. W. *J. Am. Chem. Soc.* **1998**, *120*, 11380−11390.
(11) Davies, M. S.; Berners-Price, S. J.; Hambley, T. W. *Inorg. Chem.* **2000**, *39*, 5603−5613.
(12) Legendre, F.; Bas, V.; Kozelka, J.; Chottard, J. C. *Chem.—Eur. J.* **2000**, *6*, 2002−2010.
(13) Berners-Price, S. J.; Frenkiel, T. A.; Frey, U.; Ranford, J. D.; Sadler, P. J. *J. Chem. Soc., Chem. Commun.* **1992**, 789−791.
(14) Zimmermann, T.; Leszczynski, J.; Burda, J. V. *J. Mol. Model.* **2011**, *17*, 2385−2393.
(15) Wheate, N. J.; Walker, S.; Craig, G. E.; Oun, R. *Dalton Trans.* **2010**, *39*, 8113−8127.
(16) Fichtinger-Schepman, A. M. J.; Van der Veer, J. L.; Den Hartog, J. H. J.; Lohman, P. H. M.; Reedijk, J. *Biochemistry* **1985**, *24*, 707−713.

(17) Reeder, F.; Gonnet, F.; Kozelka, J.; Chottard, J.-C. *Chem.—Eur. J.* **1996**, *2*, 1068−1076.
(18) Sadler, P. J.; Barnham, K. J.; Berners-Price, S. J.; Frey, U. *Chem.—Eur. J.* **1996**, *2*, 1283−1291.
(19) Gonnet, F.; Reeder, F.; Kozelka, J.; Chottard, J.-C. *Inorg. Chem.* **1996**, *35*, 1653−1658.
(20) Zeizinger, M.; Burda, J. V.; Leszczynski, J. *Phys. Chem. Chem. Phys.* **2004**, *6*, 3585−3590.
(21) Mantri, Y.; Lippard, S. J.; Baik, M. H. *J. Am. Chem. Soc.* **2007**, *129*, 5023−5030.
(22) Kozelka, J. *Inorg. Chim. Acta* **2009**, *362*, 651−668.
(23) Chval, Z.; Šíp, M. *Collect. Czech. Chem. Commun.* **2003**, *68*, 1105−1118.
(24) Baik, M. H.; Friesner, R. A.; Lippard, S. J. *J. Am. Chem. Soc.* **2003**, *125*, 14082−14092.
(25) Costa, L. A. S.; Hambley, T. W.; Rocha, W. R.; De Almeida, W. B.; Dos Santos, H. F. *Int. J. Quantum Chem.* **2006**, *106*, 2129−2144.
(26) Raber, J.; Zhu, C. B.; Eriksson, L. A. *J. Phys. Chem. B* **2005**, *109*, 11006−11015.
(27) Pavelka, M.; Burda, J. V. *J. Mol. Model.* **2007**, *13*, 367−379.
(28) Gao, Y.; Zhou, L. *Theor. Chem. Acc.* **2009**, *123*, 455−468.
(29) Sarmah, P.; Deka, R. C. *J. Mol. Struct. THEOCHEM* **2010**, *955*, 53−60.
(30) Zhou, L. *Inorg. Chim. Acta* **2011**, *376*, 44−56.
(31) Ranaldo, R.; Margiotta, N.; Intini, F.; Pacifico, C.; Natile, G. *Inorg. Chem.* **2008**, *47*, 2820−2830.
(32) Yang, D.; van Boom, S.; Reedijk, J.; van Boom, J.; Wang, A. *Biochemistry* **1995**, *34*, 12912−12920.
(33) Burda, J. V.; Leszczynski, J. *Inorg. Chem.* **2003**, *42*, 7162−7172.
(34) Carloni, P.; Sprik, M.; Andreoni, W. *J. Phys. Chem. B* **2000**, *104*, 823−835.
(35) Coste, F.; Malinge, J.; Serre, L.; Shepard, W.; Roth, M.; Leng, M.; Zelwer, C. *Nucleic Acids Res.* **1999**, *27*, 1837−1846.
(36) Diakos, C.; Messerle, B.; Murdoch, P.; Parkinson, J.; Sadler, P.; Fenton, R.; Hambley, T. *Inorg. Chem.* **2009**, *48*, 3047−3056.
(37) Elizondo-Riojas, M.; Kozelka, J. *J. Mol. Biol.* **2001**, *314*, 1227−1243.
(38) Gelasco, A.; Lippard, S. *Biochemistry* **1998**, *37*, 9230−9239.
(39) Gkionis, K.; Platts, J. *J. Biol. Inorg. Chem.* **2009**, *14*, 1165−1174.
(40) Jamieson, E.; Lippard, S. *Chem. Rev.* **1999**, *99*, 2467−2498.
(41) Natile, G.; Marzilli, L. G. *Coord. Chem. Rev.* **2006**, *250*, 1315−1331.
(42) Robertazzi, A.; Platts, J. A. *Chem.—Eur. J.* **2006**, *12*, 5747−5756.
(43) Saad, J.; Benedetti, M.; Natile, G.; Marzilli, L. *Inorg. Chem.* **2010**, *49*, 5573−5583.
(44) Spiegel, K.; Magistrato, A. *Org. Biomol. Chem.* **2006**, *4*, 2507−2517.
(45) Spingler, B.; Whittington, D.; Lippard, S. *Inorg. Chem.* **2001**, *40*, 5596−5602.
(46) Teletchea, S.; Skauge, T.; Sletten, E.; Kozelka, J. *Chem.—Eur. J.* **2009**, *15*, 12320−12337.
(47) Todd, R.; Lippard, S. *J. Inorg. Biochem.* **2010**, *104*, 902−908.
(48) Zayed, A.; Jones, G. D. D.; Reid, H. J.; Shoeib, T.; Taylor, S. E.; Thomas, A. L.; Wood, J. P.; Sharp, B. L. *Metallomics* **2011**, *3*, 991−1000.
(49) Chval, Z.; Šíp, M.; Burda, J. V. *J. Comput. Chem.* **2008**, *29*, 2370−2381.
(50) Chval, Z.; Šíp, M. *J. Mol. Struct. THEOCHEM* **2000**, *532*, 59−68.
(51) Tao, J.; Perdew, J.; Staroverov, V.; Scuseria, G. *Phys. Rev. Lett.* **2003**, 91.
(52) Grimme, S. *J. Comput. Chem.* **2006**, *27*, 1787−1799.
(53) Klamt, A.; Schuurmann, G. *J. Chem. Soc., Perkin Trans. 2* **1993**, 799−805.
(54) Weigend, F. *Phys. Chem. Chem. Phys.* **2006**, *8*, 1057−1065.
(55) Kabeláč, M.; Valdes, H.; Sherer, E. C.; Cramer, C. J.; Hobza, P. *Phys. Chem. Chem. Phys.* **2007**, *9*, 5000−5008.
(56) Šponer, J.; Riley, K. E.; Hobza, P. *Phys. Chem. Chem. Phys.* **2008**, *10*, 2595−2610.
(57) Mládek, A.; Šponer, J. E.; Jurečka, P.; Banáš, P.; Otyepka, M.; Svozil, D.; Šponer, J. *J. Chem. Theory Comput.* **2010**, *6*, 3817−3835.
(58) Grimme, S.; Djukic, J.-P. *Inorg. Chem.* **2011**, *50*, 2619−2628.
(59) Mutter, S. T.; Platts, J. A. *J. Phys. Chem. A* **2011**, *115*, 11293−11302.
(60) Andrae, D.; Häußermann, U.; Dolg, M.; Stoll, H.; Preuß, H. *Theor. Chem. Acc.* **1990**, *77*, 123−141.
(61) Burda, J. V.; Zeizinger, M.; Šponer, J.; Leszczynski, J. *J. Chem. Phys.* **2000**, *113*, 2224−2232.
(62) Ahlrichs, R.; Bar, M.; Haser, M.; Horn, H.; Kolmel, C. *Chem. Phys. Lett.* **1989**, *162*, 165−169.
(63) Jurečka, P.; Černý, J.; Hobza, P.; Salahub, D. R. *J. Comput. Chem.* **2007**, *28*, 555−569.
(64) Ho, J.; Klamt, A.; Coote, M. L. *J. Phys. Chem. A* **2010**, *114*, 13442−13444.
(65) Frisch, M. J.; Trucks, G. W.; Schlegel, H. B.; Scuseria, G. E.; Robb, M. A.; Cheeseman, J. R.; Scalmani, G.; Barone, V.; Mennucci, B.; Petersson, G. A.; Nakatsuji, H.; Caricato, M.; Li, X.; Hratchian, H. P.; Izmaylov, A. F.; Bloino, J.; Zheng, G.; Sonnenberg, J. L.; Hada, M.; Ehara, M.; Toyota, K.; Fukuda, R.; Hasegawa, J.; Ishida, M.; Nakajima, T.; Honda, Y.; Kitao, O.; Nakai, H.; Vreven, T.; Montgomery, Jr., J. A.; Peralta, J. E.; Ogliaro, F.; Bearpark, M.; Heyd, J. J.; Brothers, E.; Kudin, K. N.; Staroverov, V. N.; Kobayashi, R.; Normand, J.; Raghavachari, K.; Rendell, A.; Burant, J. C.; Iyengar, S. S.; Tomasi, J.; Cossi, M.; Rega, N.; Millam, J. M.; Klene, M.; Knox, J. E.; Cross, J. B.; Bakken, V.; Adamo, C.; Jaramillo, J.; Gomperts, R.; Stratmann, R. E.; Yazyev, O.; Austin, A. J.; Cammi, R.; Pomelli, C.; Ochterski, J. W.; Martin, R. L.; Morokuma, K.; Zakrzewski, V. G.; Voth, G. A.; Salvador, P.; Dannenberg, J. J.; Dapprich, S.; Daniels, A. D.; Farkas, Ö.; Foresman, J. B.; Ortiz, J. V.; Cioslowski, J.; Fox, D. J. *Gaussian 09*, Revision C.1; Gaussian, Inc.: Wallingford, CT, 2009.
(66) Keith, T. A. *AIMAll* (Version 10.11.24); TK Gristmill Software: Overland Park, KS, 2010; aim.tkgristmill.com.
(67) Glendening, E. D.; Reed, A. E.; Carpenter, J. E.; Weinhold F. *NBO 3.1*; Theoretical Chemistry Institute. University of Wisconsin: Madison, WI, 1996.
(68) Schaftenaar, G.; Noordik, J. H. *J. Comput.-Aided Mol. Des.* **2000**, *14*, 123−134.
(69) Allouche, A. *J. Comput. Chem.* **2011**, *32*, 174−182.
(70) Lu, X.; Olson, W. *Nucleic Acids Res.* **2003**, *31*, 5108−5121.
(71) Dolomanov, O.; Bourhis, L.; Gildea, R.; Howard, J.; Puschmann, H. *J. Appl. Crystallogr.* **2009**, *42*, 339−341.
(72) Alberto, M. E.; Butera, V.; Russo, N. *Inorg. Chem.* **2011**, *50*, 6965−6971.
(73) Zhang, D.; Ren, X.; Zhou, L. *Can. J. Chem.* **2010**, *88*, 1240−1246.
(74) Boys, S. F.; Bernardi, F. *Mol. Phys.* **1970**, *19*, 553−566.
(75) Zimmermann, T.; Chval, Z.; Burda, J. V. *J. Phys. Chem. B* **2009**, *113*, 3139−3150.
(76) Ziegler, T.; Rauk, A. *Theor. Chim. Acta* **1977**, *46*, 1−10.
(77) Ziegler, T.; Rauk, A. *Inorg. Chem.* **1979**, *18*, 1558−1565.
(78) Mitoraj, M.; Michalak, A.; Ziegler, T. *J. Chem. Theory Comput.* **2009**, *5*, 962−975.
(79) Mitoraj, M. P.; Zhu, H.; Michalak, A.; Ziegler, T. *Int. J. Quantum Chem.* **2009**, *109*, 3379−3386.
(80) Mitoraj, M. P.; Michalak, A.; Ziegler, T. *Organometallics* **2009**, *28*, 3727−3733.
(81) van Lenthe, E.; Baerends, E. J.; Snijders, J. G. *J. Chem. Phys.* **1993**, *99*, 4597−4610.
(82) van Lenthe, E.; van Leeuwen, R.; Baerends, E. J.; Snijders, J. G. *Int. J. Quantum Chem.* **1996**, *57*, 281−293.
(83) Laoui, A.; Kozelka, J.; Chottard, J. *Inorg. Chem.* **1988**, *27*, 2751−2753.
(84) Schneider, B.; Neidle, S.; Berman, H. *Biopolymers* **1997**, *42*, 113−124.
(85) Svozil, D.; Kalina, J.; Omelka, M.; Schneider, B. *Nucleic Acids Res.* **2008**, *36*, 3690−3706.
(86) Carlone, M.; Marzilli, L. G.; Natile, G. *Inorg. Chem.* **2004**, *43*, 584−592.

(87) Saad, J.; Natile, G.; Marzilli, L. *J. Am. Chem. Soc.* **2009**, *131*, 12314−12324.
(88) Hambley, T. W. *Inorg. Chem.* **1998**, *37*, 3767−3774.
(89) Rizzato, S.; Bergès, J.; Mason, S. A.; Albinati, A.; Kozelka, J. *Angew. Chem., Int. Ed.* **2010**, *49*, 7440−7443.
(90) Truflandier, L. A.; Sutter, K.; Autschbach, J. *Inorg. Chem.* **2011**, *50*, 1723−1732.
(91) Wu, B.; Davey, G. E.; Nazarov, A. A.; Dyson, P. J.; Davey, C. A. *Nucleic Acids Res.* **2011**, *39*, 8200−8212.
(92) Romancová, I.; Chval, Z.; Předota, M. *J. Phys. Chem. A* **2012**, *116*, 1786−1793.
(93) Wu, Y.; Bhattacharyya, D.; King, C. L.; Baskerville-Abraham, I.; Huh, S.-H.; Boysen, G.; Swenberg, J. A.; Temple, B.; Campbell, S. L.; Chaney, S. G. *Biochemistry* **2007**, *46*, 6477−6487.
(94) Sharma, S.; Gong, P.; Temple, B.; Bhattacharyya, D.; Dokholyan, N. V.; Chaney, S. G. *J. Mol. Biol.* **2007**, *373*, 1123−1140.
(95) Margiotta, N.; Marzano, C.; Gandin, V.; Osella, D.; Ravera, M.; Gabano, E.; Platts, J. A.; Petruzzella, E.; Hoeschele, J. D.; Natile, G. *J. Med. Chem.* **2012**, *55*, 7182−7192.
(96) Vrána, O.; Mašek, V.; Dražan, V.; Brabec, V. *J. Struct. Biol.* **2007**, *159*, 1−8.
(97) Šponer, J.; Sabat, M.; Gorb, L.; Leszczynski, J.; Lippert, B.; Hobza, P. *J. Phys. Chem. B* **2000**, *104*, 7535−7544.
(98) Burda, J. V.; Šponer, J.; Hrabakova, J.; Zeizinger, M.; Leszczynski, J. *J. Phys. Chem. B* **2003**, *107*, 5349−5356.
(99) Robertazzi, A.; Platts, J. *J. Biol. Inorg. Chem.* **2005**, *10*, 854−866.
(100) Robertazzi, A.; Platts, J. A. *Inorg. Chem.* **2005**, *44*, 267−274.
(101) Burda, J. V.; Šponer, J.; Leszczynski, J.; Hobza, P. *J. Phys. Chem. B* **1997**, *101*, 9670−9677.
(102) Burda, J. V.; Šponer, J.; Leszczynski, J. *Phys. Chem. Chem. Phys.* **2001**, *3*, 4404−4411.
(103) Ohndorf, U.-M.; Rould, M. A.; He, Q.; Pabo, C. O.; Lippard, S. J. *Nature* **1999**, *399*, 708−712.
(104) Sullivan, S. T.; Saad, J. S.; Fanizzi, F. P.; Marzilli, L. G. *J. Am. Chem. Soc.* **2002**, *124*, 1558−1559.
(105) Delalande, O.; Malina, J.; Brabec, V.; Kozelka, J. *Biophys. J.* **2005**, *88*, 4159−4169.
(106) Florian, J.; Brabec, V. *Chem.—Eur. J.* **2012**, *18*, 1634−1639.
(107) Jurečka, P.; Šponer, J.; Černý, J.; Hobza, P. *Phys. Chem. Chem. Phys.* **2006**, *8*, 1985−1993.
(108) Johnson, C. A.; Bloomingdale, R. J.; Ponnusamy, V. E.; Tillinghast, C. A.; Znosko, B. M.; Lewis, M. *J. Phys. Chem. B* **2011**, *115*, 9244−9251.